Chemical Engineering Journal 334 (2018) 1493–1501

Contents lists available at ScienceDirect

Chemical Engineering Journal

journal homepage: www.elsevier.com/locate/cej

Degradation of 1H-benzotriazole using ultraviolet activating persulfate: Mechanisms, products and toxicological analysis

Jinshao Ye[a,b], Pulin Zhou[a], Ya Chen[a], Huase Ou[a,*], Juan Liu[a], Chongshu Li[a], Qusheng Li[a]

[a] School of Environment, Guangdong Key Laboratory of Environmental Pollution and Health, Jinan University, Guangzhou 510632, China
[b] Joint Genome Institute, Lawrence Berkeley National Laboratory, Walnut Creek 94598, CA, USA

GRAPHICAL ABSTRACT

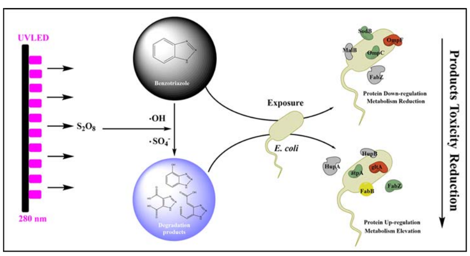

ARTICLE INFO

Keywords:
Benzotriazole
Radical oxidation
Persulfate
Photocatalysis
Proteomics

ABSTRACT

Benzotriazoles have been widely used as additives in industrial products, and they are released or discharged along with sewage into wastewater treatment plants. Traditional wastewater treatment processes, especially biological methods, cannot completely eliminate BTAs. Developing cost-effective and environmental-friendly treatment methods for the removal of benzotriazoles is in urgent need. This study evaluated the degradation efficiency of 1H-benzotriazole (1H-BTA) with 280 nm ultraviolet activating persulfate (UV/PS). Degradation of 1H-BTA followed pseudo-first order kinetics with a rate constant at 0.226 min^{-1} when $[1H\text{-}BTA]_0 = 8.39\,\mu M$, $[PS]_0 = 420\,\mu M$, UV intensity = 0.023 $mW\,cm^{-2}$. Scavenger experiments with ethanol and *tert*-butyl alcohol proved that both hydroxyl radical and sulfate radical contributed to the degradation of 1H-BTA. Reactions induced by these radicals were affected by pH value, anions and natural organic matters, implying that an incomplete mineralization of 1H-BTA by UV/PS would be ubiquitous in heterogeneous water matrix. As the reaction proceeded, 1H-BTA was transformed to a series of intermediate products. Simple hydroxylated product $C_6H_5N_3O$ was dominating in the initial stage (~10 min), while further open-loop oxidative product $C_4H_3N_3O_4$ had a peak value in the later stage (~45 min). Based on model organism proteomics and metabolic network analyses, down regulation of stress resistance proteins in *Escherichia coli* exposed to degradation products indicated that the toxicity of 1H-BTA was declined. To summarize, incomplete mineralization of 1H-BTA using UV/PS is likewise effective for its detoxification.

1. Introduction

Benzotriazoles (BTAs) are high production volume chemicals with annual output of 9000 tons worldwide [1,2], and they have been widely used as additives in industrial and household applications. A portion of BTAs is released into environment through human activity. They are considered as a category of emerging contaminants due to their persistence, bioaccumulative capacity and toxicity [3]. Residues of BTAs have been detected in sea water, river sediment and wastewater [4]. Because BTAs have high solubility (such as 1H-benzotriazole,

* Corresponding author.
E-mail address: touhuase@jnu.edu.cn (H. Ou).

https://doi.org/10.1016/j.cej.2017.11.101
Received 21 August 2017; Received in revised form 18 November 2017; Accepted 18 November 2017
Available online 21 November 2017
1385-8947/

$\sim 20\ g\ L^{-1}$), they can be transferred along with wastewater. The average concentration of BTAs in the influent of several German wastewater treatment plants (WWTPs) was $12\ \mu g\ L^{-1}$, and the effluent contained 7–18 $\mu g\ L^{-1}$ [5,6]. The BTA concentration in Switzerland wastewaters reached 100 $\mu g\ L^{-1}$ [7]. As the final step of anthropogenic water cycle, WWTPs are receptors and ultimate barriers for undesired BTAs. Removal efficiencies of different BTAs in conventional WWTPs varied from 13% to 74% [7], and it was reported that traditional treatment processes, especially biological methods, cannot completely eliminate BTAs [8]. Treated effluent containing BTAs and their degradation products is discharged into receiving water bodies from WWTPs [5,8]. Therefore, it is desirable to develop an efficient water treatment method for BTA removal.

Advanced oxidation processes (AOPs), such as ozonation [9], photocatalysis oxidation [10–12] and Fenton oxidation [13], are attempted to eliminate environmental pollutants. Among these AOPs, ultraviolet-activating persulfate (UV/$S_2O_8^{2-}$ or UV/PS) has attracted interests due to the unique advantages of sulfate radical ($\cdot SO_4^-$), such as high oxidation potential, applicability in wide pH range and much higher stability and selectivity than hydroxyl radical ($\cdot OH$) [14,15]. Similar to $\cdot OH$ oxidation, $\cdot SO_4^-$ reaction can effectively degrade familiar environmental persistent organic pollutants, such as polycyclic aromatic hydrocarbons [16], polybrominated diphenyl ethers [17,18], perfluorinated compounds [19], antibiotics [20] and disinfection by-product precursors [21,22]. Still, the research using UV/PS for BTAs degradation has only started. Several studies have proved that reaction systems containing $\cdot SO_4^-$ (without photoactivation) are efficient for BTA removal [23,24]. Ahmadi et al. [25] used a UV/TiO_2/PS system to degrade 1H-BTA, and they found that the reaction followed pseudo-first order reaction kinetics with a rate constant at 0.022 min^{-1}. However, knowledge about the degradation mechanisms and pathways are far from complete.

During the degradation of targeted contaminants (such as BTAs) with AOPs, some coexisting impurities will inhibit the degradation efficiency due to the competitive consumption of active radicals [26]. A full mineralization of targeted organic contaminant will be a great waste of energy, while an incomplete mineralization may be a proper option for UV-AOP applications, resulting in generations of numerous intermediate products. The degradation of BTAs with active radicals follows a step-by-step hydroxylation. Muller et al. [27] used ozonation to degrade several BTAs, and a series of hydroxylated, carbonylated and benzene-cleavage products were identified. In another study, Xu et al. [28] found that an opening process of the triazole ring in 1H-BTA occurred in BiOBr visible light photocatalysis, implying that different AOPs induce distinct degradation pathways. Therefore, it is important to elucidate the structure transformation and toxicity variation of BTAs degradation products during UV/PS treatments. So far, only limited information has been reported.

The existing studies in regards to the toxicological assessment of BTAs are still limited in some traditional techniques [29,30], which are primarily based on the phenotype changes of specific model organisms. For example, a luminescent bacteria experiment demonstrated that the toxicity of BTAs depends on the number, position and length of alkanes on phenyl [30]. Through *Vibrio fischeri* experiments, Borowska et al. [29] have found that direct UV photolysis can detoxify 1H-BTA solution, but it was not exactly so in a UV/H_2O_2 system. These phenotype results from the expression of a genetic code via a multi-step process can determine whether the general toxicity of a contaminant on a specific organism decreased or not, but the interactions between contaminant and biomolecules may involve the collective reactions and regulations of biomolecule replication, transcription and translation. Therefore, the toxicological evaluation of BTA degradation process will require an investigation in the perspective of protein and metabolism networks.

In the present study, the degradation kinetics and mechanism of 1H-BTA were explored using a 280 nm UV/PS system. The intermediate products were elucidated with a high resolution mass spectrometer (HRMS), while their toxicity variation was evaluated by the proteomic and metabolic network pathways in model organism *Escherichia coli*. Furthermore, influence factor experiments and a preliminary assessment of the energy consumption were performed.

2. Materials and methods

2.1. Chemical reagents and field water samples

Crystal 1H-BTA (99%, HPLC grade), ethyl alcohol (EtOH, HPLC grade), *tert*-butyl alcohol (TBA, HPLC grade) and isobaric tags for relative and absolute quantitation (iTRAQ) reagent multiplex kit (PN 4352135) were purchased from Sigma-Aldrich (USA). Analytical grade $Na_2S_2O_8$ (98%), $NaNO_3$ (98%), NaCl (98%) and humic acid (HA) (90% dissolved organic matter, CAS: 1415-93-6) were purchased from Sinopharm (China). All solutions were prepared using ultrapure water (18.2 MΩ) produced by a Milli-Q Advantage A10 system (Millipore, USA). Other chemical reagents were prepared using the highest purity available (Text S1 of the Supporting Information; "S" designates texts, tables, figures and other contents in the Supporting Information thereafter). Besides ultrapure water, four field waters were also selected as matrices for the degradation experiments. The field water samples were obtained from source water and finished water in two drinking water treatment plants (DWTPs) in Guangzhou, China. The treatment processes in these two DWTPs mainly include pre-chlorination, coagulation, sedimentation, filtration and disinfection. Detailed information about sampling and analysis procedures of these field water samples is showed in Text S2.

2.2. UV irradiation module and degradation experiments

A UV irradiation module was assembled, which consisted of an integrated 280 nm UV light emitting diode (UVLED) emission array, framework and reactor vessel (Fig. S1). Mercury lamp with 254 nm irradiation and xenon lamp with continuous wavelength irradiation (from UV to visible light) were widely applied as light sources for UV/PS reaction. Still, no research tests the effectiveness of other light sources with specific wavelengths, such as commercial UVLED emitting 280 nm irradiation. The irradiation intensity on the surface of reaction solution was set at 0.023 $mW\ cm^{-2}$. Reaction vessels were circular quartz vessels with a diameter of 12 cm. Before reaction, specific volume (typical 20 mL) of 1H-BTA solution ($[1H\text{-}BTA]_0 = 8.39\ \mu M$) was added into the reactor vessel. Initial concentration of PS was set in the range of 5–250 $mg\ L^{-1}$ (21–1050 μM). Experimental temperature was maintained at 25 ± 2 °C with pH 6.8–7.2 (if not specified otherwise). The pH value was adjusted using pH buffered solution, which contained different concentration combinations of NaOH, KH_2PO_4 and H_3PO_4. The reaction solution was persistently shaken at 60 $r\ min^{-1}$. At the pre-set times, ascorbic acid was added to scavenge persulfate. Treated sample (20 mL) was transferred into a brown amber tube at 4 °C before analysis. Control experiments using sole water, PS and UV were also performed. In the influence factor experiments, predetermined amount of NaCl (Cl^-) or $NaNO_3$ (NO_3^-) was added into the solution matrix. For HA experiments, a stock solution at 1 $g\ L^{-1}$ was prepared by adding HA into ultrapure water and filtering with 0.22 μm polyethersulfone filter. The concentrations of both NaCl and $NaNO_3$ were varied between 100–500 $mg\ L^{-1}$, while 1–50 $mg\ L^{-1}$ HA was added. Ascorbic acid was added to inhibit oxidation reaction, while EtOH and TBA were used to probe the formation of $\cdot OH$ and $\cdot SO_4^-$ in UV/PS system. Each time a single probe species was added. The concentration for EtOH, TBA and ascorbic acid were 100 mM.

2.3. Quantitative analysis of 1H-BTA and qualitative analysis of intermediate products

Quantitative analysis of 1H-BTA was conducted by a high performance liquid chromatography with a tandem mass spectrometer ($HPLC/MS^2$, TripleQuad 5500, Applied Biosystems SCIEX, USA), while determination of 1H-BTA intermediate products was performed by a TripleTOF 5600+ HRMS (Applied Biosystems SCIEX, USA). Only relative intensities (peak areas) of organic intermediate products were acquired by $HPLC/MS^2$. The molecule formula determination of generation product followed a systematic intermediate screening procedure presented in our previous study [31]. The detailed analysis procedure is presented in Text S2, Tables S1 and S2. Total organic carbon (TOC) was determined using a TOC-L analyzer (Shimadzu, Japan).

2.4. Proteomics analysis

Proteomics analysis followed four steps: (1) cells exposure to the target contaminants, (2) protein digestion, (3) peptides labeled using iTRAQ, and (4) peptides analysis using a TripleTOF 5600+ HRMS equipped with a Nanospray III source and a NanoLC 400 system (Applied Biosystems SCIEX, USA). Samples for proteomics analysis include: (1) 60 mL 8.39 μM 1H-BTA solution and (2) 60 mL UV/PS treated sample (reaction time = 20 min). The initiate reaction conditions were: temperature 25 ± 2 °C, pH 6.5–7.2, $[1H\text{-}BTA]_0$ = 8.39 μM, $[PS]_0$ = 420 μM. *Escherichia coli* ATCC11303 was selected as the model microorganism, which was inoculated in LB medium at 100 r min^{-1} for 12 h. Subsequently, the cells were obtained by centrifugation at 3500*g* for 10 min and were washed using phosphate buffered saline three times. A medium with 30 mg L^{-1} KH_2PO_4, 70 mg L^{-1} NaCl, 30 mg L^{-1} NH_4Cl, 10 mg L^{-1} $MgSO_4$, 30 mg L^{-1} beef extract, 100 mg L^{-1} peptone and 1 mg L^{-1} 1H-BTA or its intermediate mixture was prepared. The cells (0.1g L^{-1}) were inoculated into a 20 mL of this medium and shaken at 100 r min^{-1} for 24 h. After exposure, the cells were separated and washed using phosphate buffer saline for protein extraction. Detailed information about the protein digestion, iTRAQ labeling and HRMS analysis followed the same procedure described in our previous research [31].

3. Results and discussion

3.1. Basic degradation efficiency, kinetics and mineralization

It was verified that 1H-BTA was stable under UVA and UVB irradiation [18]. Thus, UVC (280 nm UVLED) was attempted in the current experiments. It was reported that high power irradiation using a medium-pressure mercury lamp (100 W, wavelength range UVB-UVC) can induce direct photolysis of 1H-BTA [29]. The irradiation intensity of UVC in this experiment (0.023 mW cm^{-2}) was far from reaching that level, the photolysis of 1H-BTA was therefore slight (removal efficiency reached ~20% within 30 min; Fig. S2). In sole water experiment, no discernible variation of 1H-BTA concentration was observed in ultrapure water solution, indicating that it is stable in pure water. Furthermore, existence of PS without any activation cannot directly degrade 1H-BTA (sole PS experiment; Fig. S2).

When UVC and PS were combined, the transformation efficiency of 8.39 μM 1H-BTA reached 99% within 30 min (Fig. 1a). Based on the fitting calculation, the decrease of 1H-BTA followed pseudo-first order kinetics, with a reaction rate constant (k_{obs}) at 0.226 min^{-1} and a half-life of 3.07 min (Fig. 1b). The initial TOC value of 8.39 μM 1H-BTA is 60.4 μg L^{-1}, and approximate 22% TOC was removed in 30 min treatment using 280 nm UV/PS (Fig. 1c), suggesting that 1H-BTA was incompletely mineralized and a variety of degradation products would be generated.

3.2. Identification of reactive radical species

The high transformation efficiency of 1H-BTA in UV/PS system may be ascribed to active radicals ($\cdot SO_4^-$ and $\cdot OH$) oxidation. Generation of $\cdot SO_4^-$ and $\cdot OH$ in UV/PS process follows these equations (Eqs. (1) and (2)) [32]:

$$S_2O_8^{2-} + h\nu \rightarrow 2\cdot SO_4^- \quad (1)$$

$$\cdot SO_4^- + OH^- \rightarrow SO_4^{2-} + \cdot OH \ (k = 7.0 \times 10^7 M^{-1} s^{-1}) \quad (2)$$

Three scavengers, i.e. ascorbic acid, EtOH and TBA, were added to probe the formation of these oxidative radicals (Fig. 1a). Removal efficiency was severely inhibited in the existence of 10 mg L^{-1} ascorbic acid, and k_{obs} decreased from 0.226 min^{-1} to 0.002 min^{-1}. Since ascorbic acid is a strong reductant and can scavenge most of the oxidants, this result suggested that the degradation of 1H-BTA is dominated by oxidation. Reaction rate constants of EtOH with $\cdot OH$ and $\cdot SO_4^-$ are 1.9×10^9 M^{-1} s^{-1} and 1.6×10^7 M^{-1} s^{-1}, respectively, while the ones of TBA with $\cdot OH$ and $\cdot SO_4^-$ are 6.0×10^8 M^{-1} s^{-1} and 4.0×10^5 M^{-1} s^{-1} [33,34]. Accordingly, EtOH scavenges both $\cdot OH$ and $\cdot SO_4^-$ with similar rate constants, while TBA is considered as the $\cdot OH$ scavenger [15]. Thus, differential degradation efficiencies in presence of EtOH and TBA can confirm the reactions of $\cdot OH$ and $\cdot SO_4^-$.

$$EtOH + \cdot OH \rightarrow products \ (k = 1.9 \times 10^9 M^{-1} s^{-1}) \quad (3)$$

$$EtOH + \cdot SO_4^- \rightarrow products \ (k = 1.6 \times 10^7 M^{-1} s^{-1}) \quad (4)$$

$$TBA + \cdot OH \rightarrow products \ (k = 6.0 \times 10^8 M^{-1} s^{-1}) \quad (5)$$

$$TBA + \cdot SO_4^- \rightarrow products \ (k = 4.0 \times 10^5 M^{-1} s^{-1}) \quad (6)$$

In the presences of EtOH and TBA, k_{obs} decreased to 0.020 min^{-1} and 0.048 min^{-1}, respectively. These results demonstrated that both $\cdot OH$ and $\cdot SO_4^-$ contributed to the degradation of 1H-BTA in 280 nm UV/PS system. Even after adding excessive EtOH, a slow degradation of 1H-BTA was still observed; besides $\cdot OH$ and $\cdot SO_4^-$ oxidation, other reaction mechanism, such as photolysis, was also involved in this UV/PS system. This is consistent with the slight decrease of 1H-BTA under sole 280 nm UV irradiation (Fig. S2).

3.3. Degradation products and their evolution pathways

Based on the proposed reaction mechanisms and the HRMS data, seven steady products, with molecular formulas of $C_6H_5N_3O$ (product A, *m/z* 136.0505), $C_6H_5N_3O_2$ (product B, *m/z* 152.0454), $C_6H_5N_3O_3$ (product C, *m/z* 168.0404), $C_5H_5N_3O_4$ (product D, *m/z* 172.0353), $C_4H_3N_3O_4$ (product E, *m/z* 158.0196), $C_6H_3N_3O_2$ (product F, *m/z* 150.0298) and $C_4H_3N_3O_3$ (product G, *m/z* 142.0247), were identified (Table S2). Some of these products were also reported previously [29].

Oxidative $\cdot SO_4^-$ and $\cdot OH$ induced a series of substitution, addition and cleavage of 1H-BTA, resulting in a transformation path of 1H-BTA, A, B, F, E (Fig. 2). Another pathway also involved oxidations and cleavages of the phenyl structure, with a generation pathway of 1H-BTA, A, B, C, D, G. These proposed pathways were verified by the variation tendencies of relative intensity (peak area; Table 1). Product A (MW, 136.0505 Da) and Product E (MW, 158.0196 Da) were the dominating intermediate products in the early and later stages, respectively. Product A has a mass of 136.0505 Da ($[M+H]^+$), which differs from $[1H\text{-}BTA+H]^+$ with a ~16 Da moiety (supposed to be a hydroxyl). It is the simplest product with a high peak intensity (1.48×10^6) at 10 min, which was supposed to be oxidized from 1H-BTA under $\cdot OH$ attack. Product E ($[M+H]^+$; 158.0196 Da) has a relative saturated and stable structure, resulting in its accumulation during the reaction. Its relative intensity reached a maximum value (3.41×10^6) at about 48 min. All these products trended to be further oxidized and finally be mineralized into H_2O and CO_2 as the reaction proceeded.

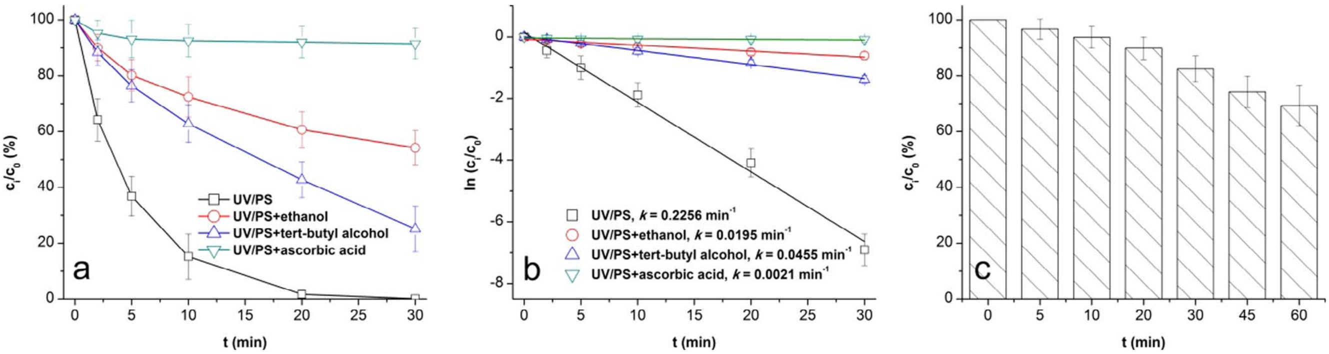

Fig. 1. Degradation efficiency, kinetics and mineralization. (a) degradation efficiency of 1H-BTA, (b) fitting of kinetics, (c) variation of total organic carbon (%). Experimental conditions: solution temperature 25 ± 2 °C, pH 6.5–7.2, $[1H\text{-}BTA]_0 = 8.39\,\mu M$, $[PS]_0 = 420\,\mu M$. All the experiments were carried out in triplicate with error bars representing the standard error of the mean.

3.4. Influence factors

Persulfate concentration is a basic factor in the UV/PS system. As the PS concentration increased from 21 μM to 1050 μM (5–250 mg L^{-1}), k_{obs} increased from 0.015 min^{-1} to 1.093 min^{-1} (Fig. S3). A nonlinear correlation was found between the PS concentration and k_{obs}. For example, when PS concentration increased from 21 μM to 105 μM, the k_{obs} only increased ~24%. The k_{obs} doubled when PS concentration increased from 105 μM to 210 μM. But in the range of 210–1050 μM, the k_{obs} increased ~25 times. Increasing PS concentration enhances the probability of molecular collision between radicals and 1H-BTA, inducing a high reaction efficiency.

Variation of pH value had a significant impact on the UV/PS system (Fig. 3a). When pH value changed from 3.0 to 9.0, the k_{obs} maintained in the range of 0.226–0.249 min^{-1}. But the k_{obs} decreased to 0.059 min^{-1} when pH value increased to 11.0, which was quarter of that at pH = 7.0. In acidic condition, $\cdot SO_4^-$ is the predominate radical [35]. As the pH value raises, the increase of OH^- leads to a transformation from $\cdot SO_4^-$ to $^\cdot OH$ (Eq. (2)), which may reduce the proportion of $\cdot SO_4^-$ in reaction system [36]. In an experiment that established a kinetic model to elucidate the mechanisms of $\cdot SO_4^-$ generation, the generation rate of $\cdot SO_4^-$ decreased under strong alkaline condition

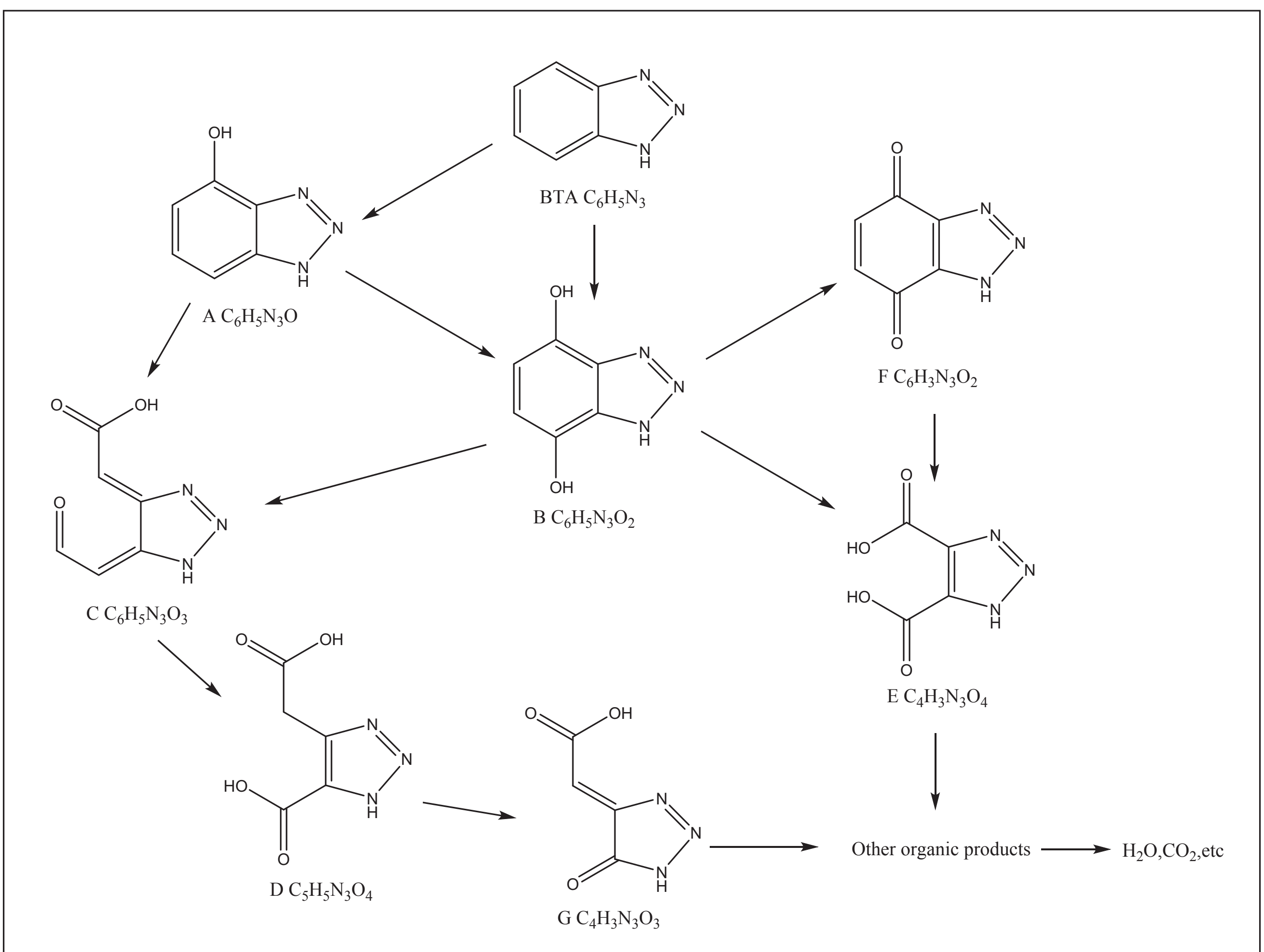

Fig. 2. Transformation pathway of 1H-BTA and its intermediate products in UV/PS system.

Table 1
Identification of 1H-BTA organic intermediates in UV/PS treatment.

Name	Product A	Product B	Product C	Product D	Evolution tendency of products A, B, C, D and G
Proposed structure	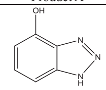	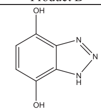	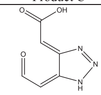	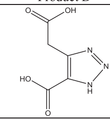	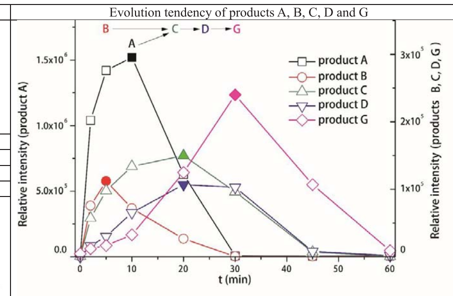
Molecular formula	$C_6H_5N_3O$	$C_6H_5N_3O_2$	$C_6H_5N_3O_3$	$C_5H_5N_3O_4$	
$[M+H]^+$: theoretical *m/z*	136.0505	152.0454	168.0404	172.0353	
$[M+H]^+$: observed *m/z*	136.0500	152.0454	168.0402	172.0349	
Retention time (min)	2.46	1.62	1.31	0.88	
Extracted ion chromatography	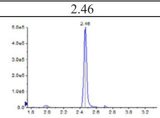	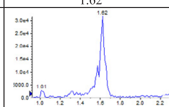	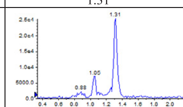	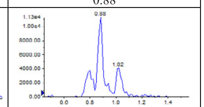	
Name	Product E	Product F	Product G		Evolution tendency of products B, E and F
Proposed structure	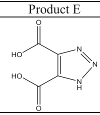	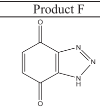	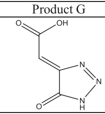		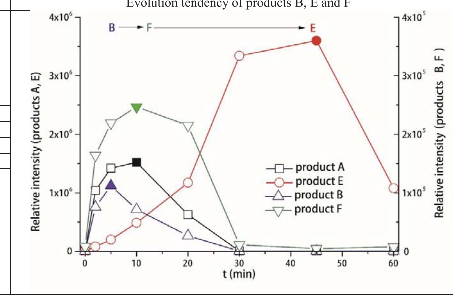
Molecular formula	$C_4H_3N_3O_4$	$C_6H_3N_3O_2$	$C_4H_3N_3O_3$		
$[M+H]^+$: theoretical *m/z*	158.0196	150.0298	142.0247		
$[M+H]^+$: observed *m/z*	158.0190	150.0297	142.0243		
Retention time (min)	1.07	2.15	1.19		
Extracted ion chromatography	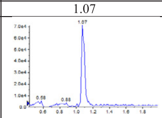	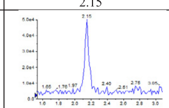	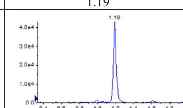		

[32]. Since ·OH (E^0 = 2.70–2.80 V) [34] has a lower oxidative capacity than $\cdot SO_4^-$ (E^0 = 2.65–3.10 V) [33], this transformation would reduce the general oxidative capacity of UV/PS system, resulting in an inhibition under strong alkaline condition. The pKa value of 1H-BTA is 8.2 [37], indicating that deprotonation of 1H-BTA occurs under strong alkaline condition. Electrostatic repulsion between negatively charged $[1H\text{-}BTA]^-$ and $\cdot SO_4^-$ will further reduce the reaction efficiency.

Degradation efficiency of 1H-BTA tended to decline in the presence of Cl^- or NO_3^- (Fig. 3). When the concentrations of Cl^- and NO_3^- increased from 0 mg L^{-1} to 500 mg L^{-1}, the k_{obs} decreased from

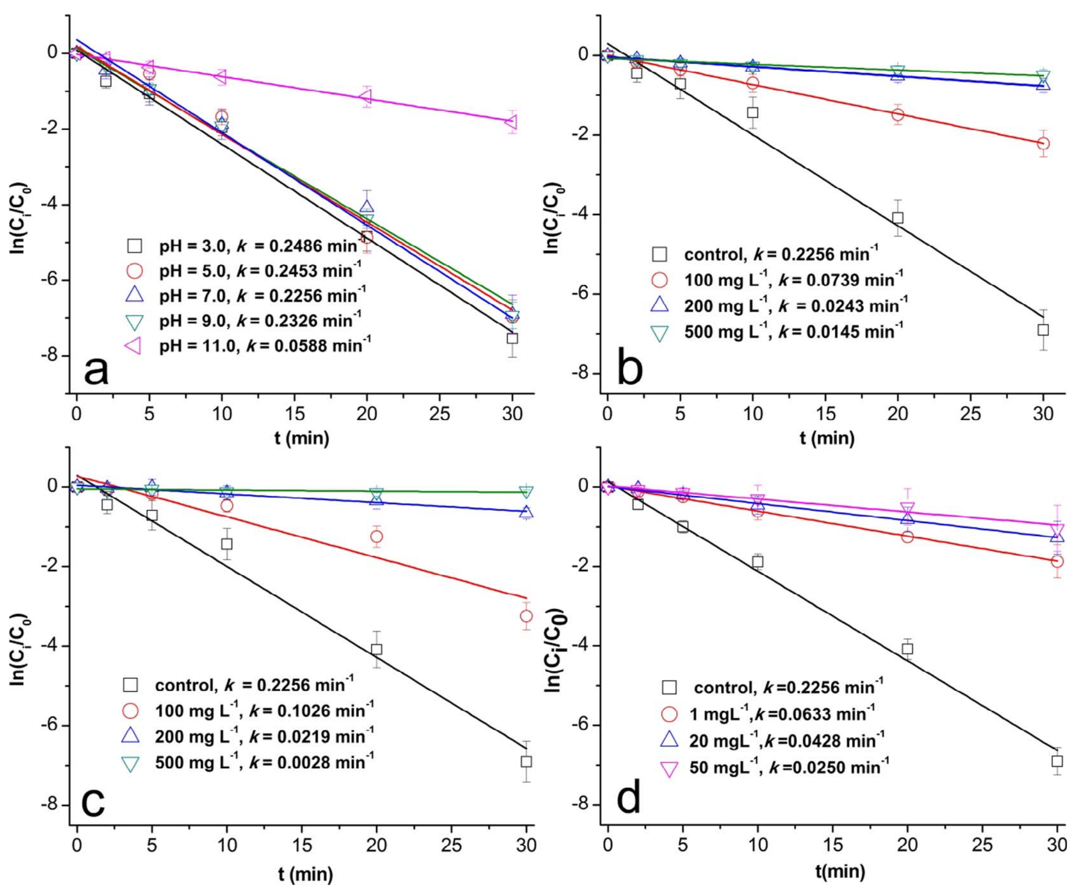

Fig. 3. Effect of different influence factors on UV/PS experiments. (a) pH value, (b) Cl^-, (c) NO_3^-, (d) humic acid. Experimental conditions: solution temperature 25 ± 2 °C, $[1H\text{-}BTA]_0$ = 8.39 μM, $[PS]_0$ = 420 μM. All the experiments were carried out in triplicate with error bars representing the standard error of the mean.

$0.226\ min^{-1}$ to $0.015\ min^{-1}$ and $0.003\ min^{-1}$, respectively. The presence of Cl^- has an inhibition on radical oxidation, which can be attributed to the transformations from $\cdot SO_4^-$ and $\cdot OH$ to less reactive oxidants $Cl\cdot$ and $\cdot OHCl^-$ (Eqs. (7) and (8)) [38,39]. As a result, the overall reaction efficiency decreased.

$$\cdot SO_4^- + Cl^- \rightarrow \cdot Cl + SO_4^{2-}\ (k = 3.1\times10^8 M^{-1}s^{-1}, pH = 6.8; [33]) \quad (7)$$

$$\cdot OH + Cl^- \rightarrow OHCl^-\ (k = 4.3\times10^9 M^{-1}s^{-1}; [34]) \quad (8)$$

The effect of NO_3^- on the UV-based reaction depends on NO_3^- concentration. Photolysis of low concentration NO_3^- ($< 10\ mg\ L^{-1}$) may produce $NO_2\cdot$ and $\cdot OH$ to enhance the degradation rate of targeted contaminant (Eqs. (9) and (10)) [40]. But high concentration NO_3^- ($> 10\ mg\ L^{-1}$) can scavenge free radicals, reducing the degradation efficiency of targeted contaminants [41]. In the current experiment, inhibition of 1H-BTA degradation was observed after adding high concentration NO_3^- (100–500 $mg\ L^{-1}$), which was attributed to the scavenging of $\cdot OH$ and/or $\cdot SO_4^-$.

$$NO_3^- \xrightarrow{h\nu} \cdot O^- + NO_2. \quad (9)$$

$$O^- + H_2O \rightarrow \cdot OH + HO^- \quad (10)$$

UV absorption may be the reason for the inhibition of UV/PS reaction. Absorbance was obtained with different concentration of Cl^-, NO_3^-, OH^- and humic acid. Strong absorbance at < 200 nm was observed in 500 $mg\ L^{-1}$ Cl^- solution. In addition, strong absorbance in the range of 200–240 nm was observed in 500 $mg\ L^{-1}$ NO_3^- and OH^- solutions. Still, very low absorbance was observed at 280 nm for NO_3^-, Cl^- and OH^-, suggesting that the inhibition of UV/PS reaction in the presents of anions (NO_3^- and Cl^-) or under alkaline condition should be attributed to other mechanisms but not UV filtering.

Concentration of HA was set at 0, 1 $mg\ L^{-1}$, 20 $mg\ L^{-1}$ and 50 $mg\ L^{-1}$. As HA concentration increased, the k_{obs} decreased from $0.226\ min^{-1}$ to $0.025\ min^{-1}$ (Fig. 3d). It can be ascribed to the capture of $\cdot SO_4^-$ and $\cdot OH$ by HA. In addition, HA can absorb UV irradiation (Fig. S4) [36,42]. Consequently, strong alkaline condition (pH ≥ 11.0), anions (Cl^- and NO_3^-) and NOM (HA) all should be paid attention to when UV/PS is applied for the degradation of 1H-BTA.

3.5. Degradation of 1H-BTA in actual water matrix

Four actual water matrixes, source water #1, source water #2, finished water #1, finished water #2, were set as background matrices (Text S2, Table S3). The k_{obs} decreased from $0.226\ min^{-1}$ to $0.138\ min^{-1}$ and $0.091\ min^{-1}$ when using two finished waters. Severe inhibitions were observed in the system using the source waters, the k_{obs} decreased to $0.014\ min^{-1}$ and $0.019\ min^{-1}$. The main distinction between source water and finished water was turbidity, while natural organic matters (NOM) and some anions (Cl^-, SO_4^{2-} and NO_3^-) in source water were higher than those in finished water. All these impurities can consume $\cdot SO_4^-$ and $\cdot OH$, resulting in lower removal efficiencies of targeted compounds [26].

3.6. Cost evaluation and quantum yield

An energy consumption assessment based on electrical energy per order (EE/O) was conducted following a similar calculation procedure reported previously [43]. EE/O only considers the electrical cost, providing reference for the evaluate the energy cost of 1H-BTA degradation using UV/PS in lab scale. Single photon energy of 280 nm UV irradiation is 7.088×10^{-19} J (4.43 eV), while the irradiation intensity on the surface of reaction solution is 0.023 $mW\ cm^{-2}$. The apparent quantum yield (Φ) under different experiment conditions were calculated following a similar procedure in Ref. [29]. In UV/PS experiment with the condition of $[1H\text{-}BTA]_0 = 8.39\ \mu M$, $[PS]_0 = 420\ \mu M$, the EE/O and Φ were 0.055 $kWh\ m^{-3}\ order^{-1}$ and 0.061 (Table S4). Generally, an increasing k_{obs} resulted in raising EE/O and declining Φ. EE/O decreased from 0.848 $kWh\ m^{-3}\ order^{-1}$ to 0.011 $kWh\ m^{-3}\ order^{-1}$ when PS concentration increased from to 21 μM to 1050 μM. For the influence factor experiments, EE/O maintained in the range of 0.050–0.055 $kWh\ m^{-3}\ order^{-1}$ when the experiment conditions were maintained in neutral and acidic, but it rose to 0.212 $kWh\ m^{-3}\ order^{-1}$ under strong alkaline condition. The existences of Cl^-, NO_3^- and HA also had impacts on the EE/O values. Degradation experiments using four actual water matrixes also presented increasing EE/O values, especially the source waters. Hence, reaction inhibitors of radicals should be paid attention to when UV/PS is applied. The EE/O value only provides information about the electrical cost. For an actual UV-based treatment process, the assessment of overall cost should take account of electrical cost, chemical reagent cost (e.g., PS addition), etc.

3.7. Differential protein expression and safety evaluation

After 20 min reaction, nearly 99% 1H-BTA was transformed to incomplete degradation products. Variations of general toxicities of 1H-BTA and degradation products were evaluated with comparing differential expression of proteins in *E. coli* ATCC11303 exposed to 1H-BTA solution after 0 and 20 min UV/PS treatment. For example, if a protein has a higher abundance (at least 1.2-fold) in the *E. coli* cells exposed to 1H-BTA compared to the cells exposed to ultrapure water (control), it is defined as an up-regulation protein.

Exposure to 1 $mg\ L^{-1}$ 1H-BTA induced the up regulations of citrate cycle, fatty acid biosynthesis, oxidative phosphorylation, pyruvate, aspartate, fructose, biotin and nucleotide metabolisms, whereas down regulations of some important reactions and pathways, including sulfur, serine and cysteine metabolisms, were also observed (Fig. S5). Several key node metabolites (phosphoribosyl diphosphate, 5-phosphoribosylamine, aminoimidazole ribotide, 5′-Phosphoribosyl-5-formamido-4-imidazolecarboxamide, inosine 5′-monophosphate and guanine) in purine metabolism pathway were synergistically up-expressed. For the up-regulated pyrimidine metabolism, it started with the increasing formation of carbamoyl phosphate from glutamine and CO_2, which is the rate-limiting step in this pyrimidine synthesis pathway catalyzed by the carbamoyl phosphate synthetase II [44]. The up-expressed aspartate carbamoyltransferase catalyzes a reaction between aspartate and carbamoyl phosphate to form N-carbamoyl-L-aspartate [45], resulting in the up-synthesis of the cytidine 5′-triphosphate and uridine 5′-triphosphate. Increasing synthesis of other related metabolites, cytidine-5′-monophosphate, uridine 5′-diphosphate, cytidine 5′-diphosphate, deoxycytidine monophosphate, etc., for nucleotide formation was also observed. Nucleotides, containing either a purine or a pyrimidine base, are the monomer units of DNA and RNA. These results all implied an up-regulation of DNA synthesis. However, RNA was down synthesized, which meant that the transcription process was inhibited by 1H-BTA.

Except for the above mentioned pathways in the metabolic network affected by 1H-BTA, some pathways related to vitamin metabolism were also differentially regulated. Among these vitamins, biotin is a water-soluble vitamin B7, which is involved in the synthesis of fatty acids, isoleucine and valine. The up expression of its whole pathway was consistent with the increasing generation of acetyl-CoA and fatty acids.

Metabolic network of *E. coli* cells exposed to 20 min degradation product mixture was dominated by down-regulated reactions and pathways. These down-regulated reactions included citrate cycle, fatty acid biosynthesis, fatty acid degradation and a series of metabolisms (pyruvate, alanine, aspartate, glutathione, threonine, etc.; Fig. 4). A small number of reactions, such as oxidative phosphorylation, glucose phosphorylation, ammonia and carbamoyl phosphate metabolisms, were up-regulated.

To further compare the differentially synthesized protein expression

Fig. 4. The KEGG metabolism network related to the different regulated expression proteins in cells under the exposure to 20-min 1H-BTA intermediate mixture. Analysis is based on the Kyoto Encyclopedia of Genes and Genomes database. Red line indicates the up-regulated metabolism pathway, while the black line indicates the down-regulated metabolism pathway.

under the exposure to intact 1H-BTA and degradation product mixture, 27 proteins with 10-fold or higher differential expression (Table 2) were selected from 717 quantifiable identified proteins (Table S5). Among these up-regulated synthesis proteins, MalB, OmpC and OmpF are membrane proteins responsible for molecule diffusion and transport [46]. These results revealed that both 1H-BTA and its degradation products can trigger the alterations of membrane-bound proteins and membrane permeability, resulting in the variations of molecule efflux and influx.

For the down regulated proteins, HupA and HupB are transcriptional regulators [47]. Their decreasing synthesis suggested a declining demand of RNA synthesis, which may be due to the detoxification of 1H-BTA after UV/PS treatment. After the exposure to 1H-BTA product mixture, the down expressions of Pgk, FabB, GapC and FabZ were observed, indicating a down-regulated pathway of fatty acid biosynthesis. However, FabB and FabZ were over produced under the stress of 1H-BTA [48]. Protein FabB uses fatty acyl thioesters of acyl-carrier protein as substrates, mediating the chain-elongation of fatty acids [49], while protein FabZ catalyzes unsaturated fatty acids biosynthesis. Their up expression under 1H-BTA stress inferred an overproduction of unsaturated long chain fatty acids.

The down expressions of several important proteins, which are responsible for stress response, were confirmed. These proteins were HdeB, UspF, Dps, SodB and DnaK (Tables 2 and S5). Protein HdeB exhibits a chaperone-like activity by preventing the aggregation of proteins [50]. In the presence of stressors, the overproduction of UspF will protect DNA [51]. In the present study, 1H-BTA induced its up regulation, whereas the degradation products of 1H-BTA decreased UspF generation, implying that 1H-BTA might be a denaturant for DNA, but its toxicity was weakened by UV/PS treatment. Protein Dps is a Fe-binding protein, which can bind the chromosome, forming a stable Dps-DNA complex to protect DNA under the stresses [52], while protein SodB can effectively destroy superoxide anion radicals which are toxic to biomolecules. Furthermore, protein DnaK assists the covalent folding or unfolding of proteins, preventing them from aggregating into non-functional structures [53]. The decreasing synthesis of transcriptional regulator proteins indicates weakening demand of DNA repair. The down expressions of stress response proteins mean bacteria or cells receive decreasing impairment from targeted contaminants. Both phenomena were observed in the *E. coli* samples exposed to 1H-BTA degradation product mixture (after 20 min UV/PS treatment), suggesting that the toxicity of 1H-BTA was declined after incomplete mineralization.

4. Conclusion

Degradation of 1H-BTA using UV/PS followed a pseudo-first order reaction. Oxidation induced by both $\cdot SO_4^-$ and $\cdot OH$ was the dominating degradation mechanism. Strongly alkaline condition inhibited the degradation efficiency, while the existences of Cl^-, NO_3^- and HA also had negative effects on the reaction. As the reaction proceeded, 1H-BTA was transformed to a series of intermediate products. Simple hydroxylated product $C_6H_5N_3O$ was dominating in the initial stage (~10 min), while further open-loop oxidative product $C_4H_3N_3O_4$ had a peak value in the later stage (~45 min). Based on the organism proteomics and metabolic network analyses, down regulation of stress resistance proteins in *Escherichia coli* exposed to degradation products indicated that their toxicity was lower than intact 1H-BTA. Incomplete hydroxylation and open loop of 1H-BTA would be ubiquitous during UV/PS treatment, and it is likewise effective for its detoxification.

Acknowledgments

This project was supported by the National Natural Science Foundation of China (Grant Nos. 51778270, 41371321), and the Fundamental Research Funds for the Central Universities (Grant No. 21617448).

Table 2
Proteins with 10-fold differential expression under the exposure to 1H-BTA or its degradation products.

Number	Accession #	Protein Name	Gene Name	Peptides (95%)	Isotope abundance comparison (1H-BTA: control*)	Isotope abundance comparison (Degradation products: control*)
1	P02943	Maltoporin	malB	30	12.7057	10.8643
2	P02931	Outer membrane protein F	ompF	29	7.3114	12.4738
3	P06996	Outer membrane protein C	ompC	15	10.1859	20.7014
4	P0AEQ1	Protein GlcG	glcG	2	13.6773	1
5	P0A6T9	Glycine cleavage system H protein	gcvH	2	7.8705	13.8038
6	P00805	L-asparaginase 2	ansB	42	0.5012	0.0608
7	P0A799	Phosphoglycerate kinase	pgk	41	0.6194	0.0308
8	P0A858	Triosephosphate isomerase	tpiA	21	1.2706	0.0488
9	P0A953	3-oxoacyl-[acyl-carrier-protein] synthase 1	fabB	27	1.3305	0.0982
10	P0ACF4	DNA-binding protein HU-beta	hupB	22	0.4207	0.0217
11	P0ACF0	DNA-binding protein HU-alpha	hupA	13	0.673	0.0649
12	P02358	30S ribosomal protein S6	rpsF	8	0.8091	0.092
13	P0AET2	Acid stress chaperone HdeB	hdeB	16	0.6668	0.0787
14	P0A6F9	10 kDa chaperonin	groS	22	0.6668	0.0711
15	P60438	50S ribosomal protein L3	rplC	7	0.871	0.0904
16	P0AFH8	Osmotically-inducible protein Y	osmY	13	0.9376	0.0565
17	P0A7R5	30S ribosomal protein S10	rpsJ	12	0.6607	0.0667
18	P0AC62	Glutaredoxin-3	grxC	4	1.2823	0.0685
19	P23857	Thiosulfate sulfurtransferase PspE	pspE	4	0.631	0.0322
20	P33898	Putative glyceraldehyde-3-phosphate dehydrogenase C	gapC	2	0.7447	0.0773
21	P60624	50S ribosomal protein L24	rplX	7	0.6918	0.0565
22	P45395	Arabinose 5-phosphate isomerase KdsD	kdsD	1	0.8318	0.0871
23	P0A6Q6	3-hydroxyacyl-[acyl-carrier-protein] dehydratase FabZ	fabZ	3	1.6444	0.0319
24	P0ACJ0	Leucine-responsive regulatory protein	lrp	1	1.4322	0.0296
25	P30850	Exoribonuclease 2	rnb	2	1.0965	0.0824
26	P00946	Mannose-6-phosphate isomerase	manA	2	1.0093	0.0313
27	P0A7T7	30S ribosomal protein S18	rpsR	4	0.5702	0.0231

* Control indicates the *E. coli* cells which exposed to distilled water without any 1H-BTA or its degradation products.

Appendix A. Supplementary data

Supplementary data associated with this article can be found, in the online version, at http://dx.doi.org/10.1016/j.cej.2017.11.101.

References

[1] S. Weiss, J. Jakobs, T. Reemtsma, Discharge of three benzotriazole corrosion inhibitors with municipal wastewater and improvements by membrane bioreactor treatment and ozonation, Environ. Sci. Technol. 40 (2006) 7193–7199.
[2] T. Ruan, R. Liu, Q. Fu, T. Wang, Y. Wang, S. Song, P. Wang, M. Teng, G. Jiang, Concentrations and composition profiles of benzotriazole UV stabilizers in municipal sewage sludge in China, Environ. Sci. Technol. 46 (2012) 2071–2079.
[3] R. Loos, B.M. Gawlik, G. Locoro, E. Rimaviciute, S. Contini, G. Bidoglio, EU-wide survey of polar organic persistent pollutants in European river waters, Environ. Pollut. 157 (2009) 561–568.
[4] S.L. Zhuang, X. Lv, L.M. Pan, L.P. Lu, Z.W. Ge, J.Y. Wang, J.P. Wang, J.S. Liu, W.P. Liu, C.L. Zhang, Benzotriazole UV 328 and UV-P showed distinct antiandrogenic activity upon human CYP3A4-mediated biotransformation, Environ. Pollut. 220 (2017) 616–624.
[5] S. Weiss, T. Reemtsma, Determination of benzotriazole corrosion inhibitors from aqueous environmental samples by liquid chromatography-electrospray ionization-tandem mass spectrometry, Anal. Chem. 77 (2005) 7415–7420.
[6] W. Giger, C. Schaffner, H.P.E. Kohler, Benzotriazole and tolyltriazole as aquatic contaminants. 1. Input and occurrence in rivers and lakes, Environ. Sci. Technol. 40 (2006) 7186–7192.
[7] D. Voutsa, P. Hartmann, C. Schaffner, W. Giger, Benzotriazoles, alkylphenols and bisphenol a in municipal wastewaters and in the Glatt River Switzerland, Environ. Sci. Pollut. Res. 13 (2006) 333–341.
[8] X. Zhao, Z.F. Zhang, L. Xu, L.Y. Liu, W.W. Song, F.J. Zhu, Y.F. Li, W.L. Ma, Occurrence and fate of benzotriazoles UV filters in a typical residential wastewater treatment plant in Harbin China, Environ. Pollut. 227 (2017) 215–222.
[9] N.K.V. Leitner, B. Roshani, Kinetic of benzotriazole oxidation by ozone and hydroxyl radical, Water Res. 44 (2010) 2058–2066.
[10] U.I. Gaya, A.H. Abdullah, Heterogeneous photocatalytic degradation of organic contaminants over titanium dioxide: a review of fundamentals, progress and problems, J. Photochem. Photobiol. C-Photochem. Rev. 9 (2008) 1–12.
[11] M.Q. Wen, T. Xiong, Z.G. Zang, W. Wei, X.S. Tang, F. Dong, Synthesis of MoS_2/g-C_3N_4 nanocomposites with enhanced visible-light photocatalytic activity for the removal of nitric oxide (NO), Opt. Express 24 (2016) 10205–10212.
[12] H. Huang, J. Zhang, L. Jiang, Z. Zang, Preparation of cubic Cu_2O nanoparticles wrapped by reduced graphene oxide for the efficient removal of rhodamine B, J. Alloys Compd. 718 (2017) 112–115.
[13] C.K. Wang, Y.H. Shih, Degradation and detoxification of diazinon by sono-Fenton and sono-Fenton-like processes, Sep. Purif. Technol. 140 (2015) 6–12.
[14] S. Wacławek, H.V. Lutze, K. Grübel, V.V.T. Padil, M. Černík, D.D. Dionysiou, Chemistry of persulfates in water and wastewater treatment: a review, Chem. Eng. J. 330 (2017) 44–62.
[15] F. Ghanbari, M. Moradi, Application of peroxymonosulfate and its activation methods for degradation of environmental organic pollutants: review, Chem. Eng. J. 310 (2017) 41–62.
[16] M. Usman, P. Faure, C. Ruby, K. Hanna, Application of magnetite-activated persulfate oxidation for the degradation of PAHs in contaminated soils, Chemosphere 87 (2012) 234–240.
[17] Y. Wang, S.-Y. Chen, X. Yang, X.-F. Huang, Y.-H. Yang, E.-K. He, S. Wang, R.-L. Qiu, Degradation of 2,2′,4,4′-tetrabromodiphenyl ether (BDE-47) by a nano zerovalent iron-activated persulfate process: the effect of metal ions, Chem. Eng. J. 317 (2017) 613–622.
[18] H.J. Peng, W. Zhang, L. Liu, K.F. Lin, Degradation performance and mechanism of decabromodiphenyl ether (BDE209) by ferrous-activated persulfate in spiked soil, Chem. Eng. J. 307 (2017) 750–755.
[19] H. Hori, A. Yamamoto, E. Hayakawa, S. Taniyasu, N. Yamashita, S. Kutsuna, Efficient decomposition of environmentally persistent perfluorocarboxylic acids by use of persulfate as a photochemical oxidant, Environ. Sci. Technol. 39 (2005) 2383–2388.
[20] J.S. Ye, J. Liu, H.S. Ou, L.L. Wang, Degradation of ciprofloxacin by 280 nm ultraviolet-activated persulfate: degradation pathway and intermediate impact on proteome of *Escherichia coli*, Chemosphere 165 (2016) 311–319.
[21] W.H. Chu, D.M. Li, N.Y. Gao, M.R. Templeton, C.Q. Tan, Y.Q. Gao, The control of emerging haloacetamide DBP precursors with UV/persulfate treatment, Water Res. 72 (2015) 340–348.
[22] W.H. Chu, T.F. Chu, T. Bond, E.D. Du, Y.Q. Guo, N.Y. Gao, Impact of persulfate and ultraviolet light activated persulfate pre-oxidation on the formation of trihalomethanes, haloacetonitriles and halonitromethanes from the chlor(am)ination of three antibiotic chloramphenicols, Water Res. 93 (2016) 48–55.
[23] W.D. Oh, S.K. Lua, Z.L. Dong, T.T. Lim, A novel three-dimensional spherical $CuBi_2O_4$ consisting of nanocolumn arrays with persulfate and peroxymonosulfate activation functionalities for 1H-benzotriazole removal, Nanoscale 7 (2015) 8149–8158.
[24] X. Xiong, B. Sun, J. Zhang, N. Gao, J. Shen, J. Li, X. Guan, Activating persulfate by Fe^0 coupling with weak magnetic field: performance and mechanism, Water Res. 62 (2014) 53–62.
[25] M. Ahmadi, F. Ghanbari, M. Moradi, Photocatalysis assisted by peroxymonosulfate and persulfate for benzotriazole degradation: effect of pH on sulfate and hydroxyl

radicals, Water Sci. Technol. 72 (2015) 2095–2102.
[26] M.C. Dodd, H.-P.E. Kohler, U. Von Gunten, Oxidation of antibacterial compounds by ozone and hydroxyl radical: elimination of biological activity during aqueous ozonation processes, Environ. Sci. Technol. 43 (2009) 2498–2504.
[27] A. Muller, S.C. Weiss, J. Beisswenger, H.G. Leukhardt, W. Schulz, W. Seitz, W.K.L. Ruck, W.H. Weber, Identification of ozonation by-products of 4- and 5-methyl-1H-benzotriazole during the treatment of surface water to drinking water, Water Res. 46 (2012) 679–690.
[28] J. Xu, L. Li, C.S. Guo, Y. Zhang, S.F. Wang, Removal of benzotriazole from solution by BiOBr photocatalysis under simulated solar irradiation, Chem. Eng. J. 221 (2013) 230–237.
[29] E. Borowska, E. Felis, J. Kalka, Oxidation of benzotriazole and benzothiazole in photochemical processes: kinetics and formation of transformation products, Chem. Eng. J. 304 (2016) 852–863.
[30] D.A. Pillard, J.S. Cornell, D.L. Dufresne, M.T. Hernandez, Toxicity of benzotriazole and benzotriazole derivatives to three aquatic species, Water Res. 35 (2001) 557–560.
[31] H.S. Ou, J. Liu, J.S. Ye, L.L. Wang, N.Y. Gao, J. Ke, Degradation of tris(2-chloroethyl) phosphate by ultraviolet-persulfate: kinetics, pathway and intermediate impact on proteome of *Escherichia coli*, Chem. Eng. J. 308 (2017) 386–395.
[32] W. Li, R. Orozco, N. Camargos, H.Z. Liu, Mechanisms on the impacts of alkalinity, pH, and chloride on persulfate-based groundwater remediation, Environ. Sci. Technol. 51 (2017) 3948–3959.
[33] P. Neta, R.E. Huie, A.B. Ross, Rate constants for reactions of inorganic radicals in aqueous-solution, J. Phys. Chem. Ref. Data 17 (1988) 1027–1284.
[34] G.V. Buxton, Critical Review of rate constants for reactions of hydrated electrons, hydrogen atoms and hydroxyl radicals ($^{\bullet}OH/^{\bullet}O^{-}$) in aqueous solution, J. Phys. Chem. Ref. Data 17 (1988) 513–886.
[35] X. He, S.P. Mezyk, I. Michael, D. Fatta-Kassinos, D.D. Dionysiou, Degradation kinetics and mechanism of β-lactam antibiotics by the activation of H_2O_2 and $Na_2S_2O_8$ under UV-254 nm irradiation, J. Hazard. Mater. 279 (2014) 375–383.
[36] Y.J. Xiao, L.F. Zhang, W. Zhang, K.Y. Lim, R.D. Webster, T.T. Lim, Comparative evaluation of iodoacids removal by UV/persulfate and UV/H_2O_2 processes, Water Res. 102 (2016) 629–639.
[37] A.R. Katritzky, S. Rachwal, G.J. Hitchings, Benzotriazole: a novel synthetic auxiliary, Tetrahedron 47 (1991) 2683–2732.
[38] P. Wang, S. Yang, L. Shan, R. Niu, X. Shao, Involvements of chloride ion in decolorization of Acid Orange 7 by activated peroxydisulfate or peroxymonosulfate oxidation, J. Environ. Sci. 23 (2011) 1799–1807.
[39] K.H. Chan, W. Chu, Degradation of atrazine by cobalt-mediated activation of peroxymonosulfate: different cobalt counteranions in homogenous process and cobalt oxide catalysts in photolytic heterogeneous process, Water Res. 43 (2009) 2513–2521.
[40] J. Mack, J.R. Bolton, Photochemistry of nitrite and nitrate in aqueous solution: a review, J. Photochem. Photobiol. A: Chem. 128 (1999) 1–13.
[41] C.Y. Wang, L.Y. Zhu, M.C. Wei, P. Chen, G.Q. Shan, Photolytic reaction mechanism and impacts of coexisting substances on photodegradation of bisphenol A by Bi_2WO_6 in water, Water Res. 46 (2012) 845–853.
[42] L.J. Bu, S.Q. Zhou, Z. Shi, L. Deng, G.C. Li, Q.H. Yi, N.Y. Gao, Degradation of oxcarbazepine by UV-activated persulfate oxidation: kinetics, mechanisms, and pathways, Environ. Sci. Pollut. Res. 23 (2016) 2848–2855.
[43] J. Ye, J. Liu, C. Li, P. Zhou, S. Wu, H. Ou, Heterogeneous photocatalysis of tris(2-chloroethyl) phosphate by UV/TiO_2: degradation products and impacts on bacterial proteome, Water Res. 124 (2017) 29–38.
[44] T. Sato, H. Akasu, W. Shimono, C. Matsu, Y. Fujiwara, Y. Shibagaki, J.J. Heard, F. Tamanoi, S. Hattori, Rheb protein binds CAD (Carbamoyl-phosphate synthetase 2, aspartate transcarbamoylase, and dihydroorotase) protein in a GTP-and effector domain-dependent manner and influences its cellular localization and carbamoyl-phosphate synthetase (CPSase) activity, J. Biol. Chem. 290 (2015) 1096–1105.
[45] I. Ben-Sahra, J.J. Howell, J.M. Asara, B.D. Manning, Stimulation of de Novo pyrimidine synthesis by growth signaling through mTOR and S6K1, Science 339 (2013) 1323–1328.
[46] V. Baldwin, M. Bhatia, M. Luckey, Folding studies of purified LamB protein, the maltoporin from the *Escherichia coli* outer membrane: trimer dissociation can be separated from unfolding, Biochim. Biophys. Acta. 2011 (1808) 2206–2213.
[47] D. Dey, V. Nagaraja, S. Ramakumar, Structural and evolutionary analyses reveal determinants of DNA binding specificities of nucleoid-associated proteins HU and IHF, Mol. Phylogenet. Evol. 107 (2017) 356–366.
[48] L. Moynie, S.M. Leckie, S.A. McMahon, F.G. Duthie, A. Koehnke, J.W. Taylor, M.S. Alphey, R. Brenk, A.D. Smith, J.H. Naismith, Structural insights into the mechanism and inhibition of the beta-Hydroxydecanoyl-Acyl carrier protein dehydratase from *Pseudomonas aeruginosa*, J. Mol. Biol. 425 (2013) 365–377.
[49] Y. Zhang, C. Rock, Membrane lipid homeostasis in bacteria, Nat. Rev. Microbiol. 6 (2008) 222–233.
[50] J.U. Dahl, P. Koldewey, L. Salmon, S. Horowitz, J.C.A. Bardwell, U. Jakob, HdeB Functions as an acid-protective chaperone in bacteria, J. Biol. Chem. 290 (2015) 65–75.
[51] Q. Jia, X. Hu, D. Shi, Z. Yan, M. Sun, J. Wang, K. Mi, G. Zhu, Corrigendum: universal stress protein Rv2624c alters abundance of arginine and enhances intracellular survival by ATP binding in mycobacteria, Sci. Rep. 6 (2016) 35462.
[52] A.R. Arnold, A. Zhou, J.K. Barton, Characterization of the DNA-Mediated Oxidation of Dps a bacterial ferritin, J. Am. Chem. Soc. 138 (2016) 11290–11298.
[53] F. Anglès, M.P. Castaniécornet, N. Slama, M. Dinclaux, A.M. Cirinesi, J.C. Portais, F. Létisse, P. Genevaux, Multilevel interaction of the DnaK/DnaJ(HSP70/HSP40) stress-responsive chaperone machine with the central metabolism, Sci. Rep. 7 (2017) 41341.